Università degli Studi di Bari Aldo Moro

FACOLTÀ DI SCIENZE MATEMATICHE, FISICHE E NATURALI

CORSO DI LAUREA MAGISTRALE IN FISICA

titolo

Relatore:
Dott.ssa Anna Colaleo

Laureando:
Filippo Errico

ANNO ACCADEMICO 2013-2014

Contents

Introduction

Il Modello Standard (MS) delle interazioni fondamentali è una delle teoria più dibattute degli ultimi anni ed ha ottenuto nell'ultimo secolo numerose conferme sperimentali, con altissimi livelli di precisione. L'ultimo pezzo mancante per la conferma della teoria è stato per un lungo periodo il bosone di Higgs, il quanto del campo scalare ritenuto responsabile della rottura spontanea della simmetria di *gauge* del MS. Grazie a questo meccanismo tutte le particelle elementari acquistano massa.
La massa del bosone di Higgs è un parametro libero della teoria e può variare in un ampio intervallo di valori. Numerosi esperimenti hanno cercato segni della sua esistenza, ma sono riusciti solo ad escludere alcuni intervalli di massa. Il *Large Hadron Collider* (LHC) è l'acceleratore di particelle costruito per investigare la rottura spontanea della simmetria e riuscire a dare una prova definitiva dell'esistenza del bosone di Higgs.

Chapter 1

The Standard Model and beyond

Particle Physics studies the building blocks of the matter, the so called fundamental particle, and how they are governed by the four fundamental forces[1].
The best theory, explaining our understanding of these particles and forces, is the *Standard Model* (SM): developed during the 1970s, it has successfully explained almost all experimental results and precisely predicted a wide variety of physical phenomena.
This chapter will describe in details the Standard Model and some theories developed in order to solve some unanswered questions.

1.1 The Standard Model

1.1.1 Fundamental Particles

All matter around us is made of elementary particles, the building blocks of matter. These particles are divided into two groups: *leptons*, with an entire value of electric charge, and *quarks*, with a fractional charge. Each group consists of six particles, which are related in pairs, or generations. The six quarks are paired in the three generations: the up quark and the down quark form the first generation, followed by the charm quark and strange quark, then the top quark and bottom (or beauty) quark. The six leptons are similarly arranged in three generations: the electron and the electron neutrino, the muon and the muon neutrino, and the tau and the tau neutrino. While electron, muon and tau are charged particles, the neutrinos are electrically neutral. In Table 1.1 and 1.2, the features of leptons and quarks.

Beside these leptons and quarks, there are other particles responsible of carrying the fundamental forces, the so called *bosons*. The Electromagnetic Force, responsible of all eletrical and magnetic phenomena, is mediated by the phtons γ; the Weak Force, responsible of some decays, is mediate by $W^{\pm}$ and Z bosons; the Strong Force, responsible for example of the atomic structure, is mediated by the gluons (g). Last fundamental

[1] In the thesis, Natural Units will be used: $c = \hbar = 1$, where $\hbar = h/2\pi = 6.58211889(26) \cdot 10^{-23} MeVs$ and $c = 299792458\ ms^{-1}$.

Leptons		
Flavor	Charge	Mass[MeV]
neutrino e. (ν_e)	0	< 0.002
electron (e)	-1	0.511
neutrino mu (ν_μ)	0	< 0.19
muon (μ)	-1	105.66
neutrino tau (ν_τ)	0	< 18.2
tau (τ)	-1	1776.86±0.12

Table 1.1: Standard Model leptons features [1].

Quark		
Flavor	Carica	Massa[GeV]
up (u)	+2/3	$0.0022^{+0.0006}_{-0.0004}$
down (d)	-1/3	$0.0047^{+0.0005}_{-0.0004}$
charm (c)	+2/3	1.28 ± 3
strange (s)	-1/3	0.096 ± 0.084
top (t)	+2/3	173.1 ± 0.6
bottom (b)	-1/3	$4.18^{+0.04}_{-0.03}$

Table 1.2: Standard Model quarks features [1].

force, not yet included in the SM, is the Gravity that is the weakest. In Table 1.3 the features of the bosons.

Bosons	Interaction	Charge	Mass[GeV]
photon (γ)	Electromagnetic	0	0
$W^\pm$	Weak	±1	80.385±0.015
Z^0	Weak	0	91.1876±0.0021
gluoni	Strong	0	0

Table 1.3: Standard Model bosons features [1].

1.1.2 Gauge Symmetries

The present belief is that all particles interactions may be dictated by the so called *local gauge symmetries* and this is connected with the idea that the conserved physical quantities (such as electric charge) are conserved in local regions of space and not just globally[2].

The fundamental quantity in classical mechanics is the action S, the time integral of the Lagrangian L:

$$S = \int L\, dt = \int \mathcal{L}(\phi, \partial\phi/\partial x_\mu)\, d^4x \tag{1.1}$$

where $\mathcal{L}$ is the Lagrangian Density[2], and ϕ is the filed, itself a function of the continuous parameters x_μ [3][4]. The *principle of least action* states that fixed the values of the coordinates at the initial time t_{in} and at the final time t_f, then classical trajectory which satisfies these conditions is an extremum of the action. This leads to the *Euler-Lagrange* equations (1.2) from which can be obtained the particle equations of motion.

$$\frac{\partial\mathcal{L}}{\partial\phi} - \frac{\partial}{\partial x_\mu}\frac{\partial\mathcal{L}}{\partial(\partial\phi/\partial x_\mu)} = 0 \tag{1.2}$$

QED

The interaction of electron with photon is described by the Quantum Electrodynamics. Let's start with a complex field ψ describing a free electron with mass m: its Lagrangian is

$$\mathcal{L} = \bar{\psi}(i\gamma^\mu\partial_\mu - m)\psi \tag{1.3}$$

and its equation of motion can be deduced by the Dirac Equation, obtained substituting 1.3 in 1.2.
The electromagnetic (em) field instead is described by a four-vector A_μ, the gauge potential. The field strength tensor is defined as:

$$F_{\mu\nu} = \partial_\mu A_\nu - \partial_\nu A_\mu \tag{1.4}$$

and the equation of motion, in presence of an external current J^μ is:

$$\partial_\mu F^{\mu\nu} = QeJ^\nu \tag{1.5}$$

In case now the electron interacts with the em field, the new Lagrangian is:

$$\mathcal{L}_{EM} = \bar{\psi}(i\gamma^\mu D_\mu - m)\psi - \frac{1}{4}F_{\mu\nu}F^{\mu\nu} \tag{1.6}$$

where D_μ, known as covariant derivative, is defined as

$$D_\mu = \partial_\mu + ieQA_\mu \tag{1.7}$$

and the last term in 1.6 stands for Maxwell's equation.
It can be shown that 1.6 is invariant under the phase transformation:

$$\psi(x) \to e^{-iQ\theta}\psi(x) \tag{1.8}$$

with $\theta \in \Re$. This transformation belongs to the group U(1) and according to Noether's theorem, it implies the existence of a conserved current: the electric charge. In this case,

[2]however, following standard use in field theory, we will often refer to $\mathcal{L}$ simply Lagrangian.

known as *global "gauge" invariance*, once the value of θ is fixed, it is specified for all space and time.
More interesting is the case in which the parameter θ depends on space and time in a completely arbitrary way:

$$\psi(x) \to e^{-iQ\theta(x)}\psi(x) \tag{1.9}$$

and the Lagrangian 1.6 is not invariant. It can be shown that, in oder to restore the Lagrangian invariance, the potential A_μ must satisfy following condition:

$$A_\mu \to A_\mu + \frac{1}{e}\partial_\mu\theta \tag{1.10}$$

Under 1.9 and 1.10 the Lagrangian 1.6 is invariant.
One can observe the absent of mass term in the Lagrangian: this means that the boson associated to the potential A_μ, the photon, must be massless: the presence of a mass term would make the Lagrangian not invariant under gauge transformation.

QCD

The interaction between quarks and gluons is described by the Quantum Chromodynamics.
For quarks [5], it must be considered a new quantum number, the colour, such that each species of quark may have three different colours: $q_j,\ j = 1, 2, 3$ (red, green, blue). In order to avoid the existence of non-observed extra states with non-zero colour, one needs to further postulate that all asymptotic states are colourless, i.e. singlets under rotations in colour space. This assumption is known as the confinement hypothesis, because it implies the non-observability of free quarks: since quarks carry colour they are confined within colour-singlet bound states.
For free quark described by the field q_j, the Lagrangian is:

$$\mathcal{L} = \bar{q_j}(i\gamma^\mu\partial_\mu - m)q_j \tag{1.11}$$

In order to describe the interaction between quarks and gluons, it is needed to change the quark derivative by covariant objects. Since there are now eight independent gauge parameters, eight different gauge bosons $G_a^\mu(x)$, the so-called gluons, are needed:

$$D_{q_f}^\mu \equiv [\partial^\mu - ig_s\frac{\lambda^a}{2}G_a^\mu(x)] \tag{1.12}$$

The corresponding field strengths are also introduced:

$$G_a^{\mu\nu} = \partial^\mu G_a^\nu - \partial^\nu G_a^\mu + g_s f^{abc} G_b^\mu G_c^\nu \tag{1.13}$$

where g_s is the constant coupling. Hence, in case of interaction the new Lagrangian is:

$$\mathcal{L}_{QCD} = \bar{q_j}(i\gamma^\mu D_\mu - m)q_j - \frac{1}{4}G_a^{\mu\nu}G_{\mu\nu}^a \tag{1.14}$$

It can be shown 1.14 in invariant under arbitrary global $SU(3)_C$ transformations in colour space 1.15:

$$q(x) \to q'(x) = Uq(x) \equiv e^{i\theta_a T^a} q(x), \quad a = 1, 2, ..., 8 \tag{1.15}$$

where T_a are the generators of the SU(3) (n = $N^2 - 1 = 3^2 - 1 = 8$) group linked with the λ_a Gell-Mann matrices.
More interesting is the case in which θ depends on local coordinates, $\theta_a = \theta_a$(x):

$$q(x) \to q'(x) = Uq(x) \equiv e^{i\theta_a(x)\frac{\lambda^a}{2}} q(x), \quad a = 1, 2, ..., 8 \tag{1.16}$$

The group is non-Abelian since not all the generators λ_a commute with each other.
To ensure the invariance of the Lagrangian 1.14, the gauge fields must transform as follow:

$$G^a_\mu \to G^a_\mu - \frac{1}{g_s}\partial_\mu \theta_a - f_{abc}\theta^b G^c_\mu \tag{1.17}$$

The field tensor $G^{\mu\nu}_a$ has a remarkable new property: imposing gauge symmetry (1.16 and 1.17) has required that the kinematic energy term in 1.14 in not purely kinetic but includes an induced self-interaction between the gauge bosons. Decomposing the Lagrangian into its different pieces, there are three terms analogues to QED describing the free propagation of quarks and gluons and the quark-gluon interaction. The remaining two terms show the presence of three and four gluon self-coupling in QCD and reflect the fact that gluons themselves carry color charge. They have no analogue in QED and arise on account of the non-Abelian character of the gauge group. As in QED, the absence of a mass term implies gluons must be massless.

The electroweak theory

Low-energy experiments have provided a large amount of information about the dynamics underlying flavour-changing processes. The detailed analysis of the energy and angular distributions in β decays, such as $\mu^- \to e^- \bar{\nu}_e \nu_\mu$, made clear that only the left-handed (right-handed) fermion (antifermion) chiralities participate in those weak transitions. Moreover, the strength of the interaction appears to be universal.
Using gauge invariance, it is possible to determine the right QED (1.1.2 and QCD 1.1.2 Lagrangians. To describe weak interactions, a more elaborated structure is needed, with several fermionic flavours and different properties for left- and right-handed fields. Moreover, the left-handed fermions should appear in doublets, and we would like to have gauge bosons in addition to the photon. The simplest group with doublet representations is SU(2) while to include also the electromagnetic interactions an additional U(1) group is needed. The obvious symmetry group to consider is then:

$$G \equiv SU(2)_L \otimes U(1)_Y \tag{1.18}$$

where L refers to left-handed fields and Y stands for the weak hypercharge.
Let's consider a single family of leptons:

$$\chi_L = \begin{pmatrix} \nu_l \\ l^- \end{pmatrix}_L, \quad \psi_R = l_R^- \tag{1.19}$$

or for quarks

$$\chi_L = \begin{pmatrix} u \\ d \end{pmatrix}_L, \quad \psi_R = u_R, \ or \ d_R \tag{1.20}$$

As in QED and QCD case, starts with free Lagrangian:

$$\mathcal{L} = i\bar{\chi}_L \gamma^\mu \partial_\mu \chi_L + i\bar{\psi}_R \gamma^\mu \partial_\mu \psi_R \tag{1.21}$$

The interaction is again introduced changing the derivative with the covariante:

$$D_\mu = \partial_\mu + igW_\mu^a T^a + ig' B_\mu Y \tag{1.22}$$

where W_μ^a a = 1, 2, 3 are the three gauge bosons associated with the group $SU(2)_L$, T^a its generators and g the constant couplings; B_μ, Y and g are instead respectively the gauge boson, the generator and the constant coupling for the group $U(1)_Y$. With W_μ^a and B_μ can be introduced also the tensor strength fields:

$$\begin{aligned} W_a^{\mu\nu} &= \partial^\mu W_a^\nu - \partial^\nu W_a^\mu + g\epsilon^{abc} W_b^\mu W_c^\nu \\ B^{\mu\nu} &= \partial^\mu B^\nu - \partial^\nu B^\mu \end{aligned} \tag{1.23}$$

Therefore, the properly Lagrangian is given by:

$$\mathcal{L} = i\bar{\chi}_L \gamma^\mu D_\mu \chi_L + i\bar{\psi}_R \gamma^\mu D_\mu \psi_R - \frac{1}{4} B_{\mu\nu} B^{\mu\nu} - \frac{1}{4} W_{\mu\nu} W^{\mu\nu} \tag{1.24}$$

In 1.24 $W_{\mu\nu} = W_{\mu\nu}^a \sigma^a / 2$ with σ^a 2x2 Pauli's matries.
As in QED and QCD case, also electroweak interaction is invariant under global transformation:

$$\begin{aligned} \chi_L \to \chi_L' &= e^{i\alpha_a T^a + i\beta Y} \chi_L \\ \psi_R \to \psi_R' &= e^{i\beta Y} \psi_R \end{aligned} \tag{1.25}$$

Moving to local transformation, in order to guarantee Lagrangian 1.24 to be invariant, the gauge bosons must have following transformation rules:

$$\begin{aligned} W_\mu^a &\to U_L(x) W_\mu^a \frac{\sigma_a}{2} U_L(x)^\dagger - \frac{i}{g} \partial_\mu U_L(x) U_L(x)^\dagger, \\ B_\mu &\to B_\mu + \frac{1}{g'} \partial_\mu \beta \end{aligned} \tag{1.26}$$

where $U(x)_L = e^{i\sigma_a/2 \ \alpha(x)^a}$. The transformation of B_μ is identical to the one obtained in QED for the photon, while the $SU(2)_L$ W_μ^a fields transform in analogous way to the

gluon fields of QCD.
The gauge symmetry forbids to write a mass term for the gauge bosons in 1.24. Fermionic masses are also not possible, because they would communicate the left- and right-handed fields, which have different transformation properties, and therefore would produce an explicit breaking of the gauge symmetry. Thus, the $SU(2)_L \otimes U(1)_Y$ Lagrangian in 1.24 only contains massless fields.
The term containing the $SU(2)_L$ matrix:

$$\frac{\sigma^a}{2} W_\mu^a = \frac{1}{\sqrt{2}} \begin{pmatrix} \sqrt{2}W_\mu^3 & W_\mu^+ \\ W_\mu^- & -\sqrt{2}W_\mu^3 \end{pmatrix} \tag{1.27}$$

gives rise to charged-current interactions with the bosons field $W_\mu^\pm \equiv (W_\mu^1 \mp iW_\mu^2)/\sqrt{2}$. La Lagrangian 1.24 contains also interactions with the neutral gauge field W_μ^3 and B_μ; one can define

$$Z_\mu = \frac{gW_\mu^3 - g'B_\mu}{\sqrt{g^2 + g'2}}, \quad A_\mu = \frac{gW_\mu^3 + g'B_\mu}{\sqrt{g^2 + g'2}} \tag{1.28}$$

and thinking them as a rotation, introducing the Weinberg angle θ_W so that $\cos\theta_W = g/\sqrt{g^2 + g'2}$ (and $\sin\theta_W = g'/\sqrt{g^2 + g'2}$):

$$Z_\mu = \cos\theta_W W_\mu^3 - \sin\theta_W B_\mu, \quad A_\mu = \sin\theta_W W_\mu^3 + \cos\theta_W B_\mu \tag{1.29}$$

or reversing:

$$\begin{pmatrix} W_\mu^3 \\ B_\mu \end{pmatrix} \equiv \begin{pmatrix} \cos\theta_W & \sin\theta_W \\ -\sin\theta_W & \cos\theta_W \end{pmatrix} \begin{pmatrix} Z_\mu \\ A_\mu \end{pmatrix} \tag{1.30}$$

With these definitions, it can be observed the A_μ in1.24 couple in the same way with l_L and l_R as the photon: to get QED from these one needs to impose

$$g \sin\theta_W = g' \cos\theta_W = e \tag{1.31}$$

At the same time, Z_μ, can be identify with the Z boson, mediator of the Weak Interaction.
Once again, no mass term is present in 1.24 and this means that $W^\pm$ and Z must be massless: this is in contrast with experimental evidence [6][7].
The way to generate the mass of the particle is through the so called *Spontaneous Symmetry Breaking* (SSB): this mechanism appear in those cases where one has a symmetric Lagrangian, but a non-symmetric vacuum.

1.1.3 Spontaneous Symmetry Breaking and the Higgs Boson

Let's consider a complex scalar field $\phi(x) = (\phi_1 + \phi_2)/\sqrt{2}$, with Lagrangian:

$$\mathcal{L} \equiv T - V = (\partial_\mu \phi)^* (\partial^\mu \phi) - \mu^2(\phi^*\phi) - \lambda(\phi^*\phi)^2 \tag{1.32}$$

1.32 is invariant under global phase transformation of the scalar field (it possesses a U(1) global gauge symmetry).
Considering the case when $\lambda > 0$, for the quadratic piece there are two possibilities:

- $\mu^2 > 0$: the potential has only the trivial minimum $\phi = 0$
- $\mu^2 < 0$: the minimum is every point belong to the circle (in the ϕ_1, ϕ_2) of radius ν such that:

$$(\phi_1)^2 + (\phi_2)^2 = \nu^2 \quad with\ \nu^2 = -\frac{\mu^2}{\lambda} \tag{1.33}$$

as shown in Figure 1.1

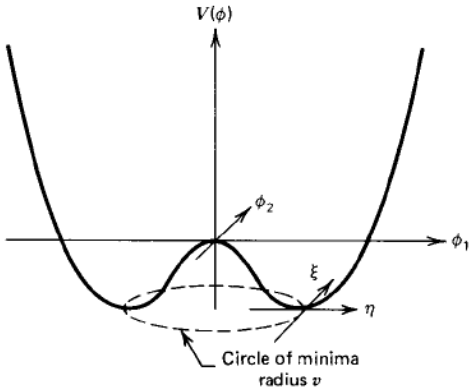

Figure 1.1: The potential $V(\phi)$ for a complex scalar field with $\lambda > 0$ and $\mu^2 < 0$.

Owing to the U(1) phase-invariance of the Lagrangian 1.32, there is an infinite number of degenerate states of minimum energy. By choosing a particular solution, $\phi_1 = \nu$ and $\phi_2 = 0$, as the ground state, the symmetry gets spontaneously broken. Parametrising the excitations over the ground state as:

$$\phi(x) \equiv \frac{1}{\sqrt{2}}[\nu + \eta(x) + i\xi(x)] \tag{1.34}$$

and substituting into 1.32, one obtains:

$$\mathcal{L}' = \frac{1}{2}(\partial_\mu \xi)^2 + \frac{1}{2}(\partial_\mu \eta)^2 + \mu^2\eta^2 + const. + O(\eta^3) + O(\xi^3) \tag{1.35}$$

The third term has the form of a mass term for η-field: the η-mass is $m_\eta = \sqrt{-2\mu^2}$. The first term in 1.35 represents the kinetic energy of the ξ-field but there is no corresponding mass term for the ξ. The fact there are massless excitations associated with the SSB mechanism is completely general result, known as the *Goldstone theorem*: if a Lagrangian is invariant under a continuous symmetry group G, but the vacuum is only invariant under a subgroup $H \subset G$, then there must exist as many massless spin-0 particles (Goldstone bosons) as broken generators (i.e., generators of G which do not belong to H).

The Higgs Mechanism

Let's move to consider the case for spontaneous breaking of U(1) local gauge symmetry. Taking into account the covariant derivative 1.7 where the gauge filed transforms as in 1.10, the new Lagrangian can be written as

$$\mathcal{L} = D^{\mu}\phi^{*}D_{\mu}\phi - \mu^{2}\phi^{*}\phi - \lambda(\phi^{*}\phi)^{2} - \frac{1}{4}F_{\mu\nu}F^{\mu\nu} \tag{1.36}$$

If $\mu^2 > 0$, 1.36 is just the QED Lagrangian for a charged scalar particle of mass μ. For the case $\mu^2 < 0$, it is interesting to note that to lowest oder in ξ, 1.34 can be expressed as

$$\phi(x) \equiv \frac{1}{\sqrt{2}}[\nu + \eta(x)]e^{i\xi(x)/\nu} \tag{1.37}$$

and this suggests to use different set of real field: h, θ, A_μ where now

$$\begin{aligned} \phi(x) &\rightarrow \frac{1}{\sqrt{2}}[\nu + h(x)]e^{i\theta(x)/\nu}, \\ A_\mu &\rightarrow A_\mu + \frac{1}{e\nu}\partial_\mu\theta \end{aligned} \tag{1.38}$$

This is a particular choice of gauge, with $\theta(x)$ chosen so that h is real. Substituting 1.38 in 1.36, one obtains:

$$\begin{aligned} \mathcal{L}' =& \frac{1}{2}(\partial_\mu h)^2 - \lambda\nu^2 h^2 + \frac{1}{2}e^2\nu^2 A_\mu^2 - \lambda\nu h^3 - \frac{1}{4}\lambda h^4 \\ &+ \frac{1}{2}e^2 A_\mu^2 h^2 + \nu e^2 A_\mu^2 h - \frac{1}{4}F_{\mu\nu}F^{\mu\nu} \end{aligned} \tag{1.39}$$

The Goldstone boson does not appear in the theory. That is because it corresponding only to the freedom to make a gauge transformation. The Lagrangian 1.39 describes just two interacting massive particles, a vector gauge bosoon A_μ and a massive scalar h, which is called a *Higgs particle*. This is called the "*Higgs mechanism*".
Consider now the case of $SU(2)_L \otimes U(1)_Y$ symmetry [8] with the Lagrangian

$$\mathcal{L} = (D_\mu\phi)^{\dagger}(D^\mu\phi) - \mu^2\phi^{\dagger}\phi - \lambda(\phi^{\dagger}\phi)^2 \tag{1.40}$$

D_μ is the covariant derivative 1.22 and ϕ is an SU(2) doublet of complex scalar fields:

$$\phi(x) \equiv \begin{pmatrix} \phi^{+}(x) \\ \phi^{0}(x) \end{pmatrix} \tag{1.41}$$

1.40 is invariant under local $SU(2)_L \otimes U(1)_Y$ transformations.
In $\mu^2 < 0$ and $\lambda^2 > 0$ conditions, to generate gauge boson masses, a vacuum expectation value of $\phi(x)$ must be chosen:

$$\phi_0 \equiv \frac{1}{\sqrt{2}}\begin{pmatrix} 0 \\ \nu \end{pmatrix} \tag{1.42}$$

In this way, the symmetry is broken and this generates a mass for the corresponding gauge boson. This particular choice of ϕ_0 breaks both $SU(2)$ and $U(1)_Y$ gauge symmetries but since it is neutral, the $U(1)_{em}$ remains unbroken and this means the photon remains massless.
Now, substituting the vacuum expectation value ϕ_0 for $\phi(x)$ in the Lagrangian 1.40, the expression for W and Z bosons mass are:

$$M_W^2 = \frac{\nu^2 g^2}{4}, \quad M_Z^2 = \frac{\nu^2 g^2}{4\cos^2\theta_W} = \frac{M_W^2}{\cos^2\theta_W} \tag{1.43}$$

From experimental observation [1]:

$$M_Z = XXX \pm 0XXX\ GeV, \quad M_W = XXX \pm XX\ GeV \tag{1.44}$$

From these experimental numbers, one obtains the electroweak mixing angle:

$$\sin^2\theta_W = 1 - \frac{M_W^2}{M_Z^2} = XXXX \tag{1.45}$$

The scalar vacuum expectation value is:

$$\nu = (\sqrt{2}G_F)^{-1/2} = 246\ GeV \tag{1.46}$$

where $G_F = \text{XXXXX}$ is the Fermi coupling whose value can be measured with the muon lifetime [9].
From 1.40, the potential $V(\phi)$ can be seen as:

$$V(\phi) = -\frac{1}{4}\lambda\nu^2 + V_H + V_{HG^2} \tag{1.47}$$

The first term stands for mass of the new Higgs boson: $m_H = \sqrt{2\lambda\nu^2}$; the second represents Higgs boson self-interaction and the last the coupling with the weak bosons (W and Z).
It is interesting to note the same Higgs doublet which generates weak bosons masses can give masses also to leptons and quarks. In particular, let's consider the following Lagrangian:

$$\mathcal{L} = -G_e[(\bar{\nu}_e,\ \bar{e})_L \begin{pmatrix}\phi^+\\ \phi^0\end{pmatrix} e_R + \bar{e}_R(\phi^-,\ \bar{\phi}^0)\begin{pmatrix}\nu_e\\ e\end{pmatrix}_L] \tag{1.48}$$

Substituting the expression of ϕ:

$$\phi = \frac{1}{\sqrt{2}}\begin{pmatrix}0\\ \nu + h(x)\end{pmatrix} \tag{1.49}$$

into 1.48, the Lagrangian becomes:

$$\mathcal{L} = -\frac{G_e}{\sqrt{2}}\nu(\bar{e}_L e_R + \bar{e}_R e_L) - \frac{G_e}{\sqrt{2}}h(\bar{e}_L e_R + \bar{e}_R e_L) \tag{1.50}$$

Choosing G_e so that $m_e = G_e\nu/\sqrt{2}$, since the G_e is arbitrary, the actual mass of the electron is not predicted.
The quark masses are generated in the same way with the difference that to generate a mass for the upper member of a quark doublet, a new Higgs doublet from ϕ must be used:

$$\phi_c = i\tau\phi^* = \begin{pmatrix} -\bar{\phi}^0 \\ \phi^- \end{pmatrix} \xrightarrow[breaking]{} \frac{1}{\sqrt{2}} \begin{pmatrix} \nu + h(x) \\ 0 \end{pmatrix} \tag{1.51}$$

The new Lagrangian can be written as:

$$\mathcal{L} = -G_d(\bar{u},\ \bar{d})_L \begin{pmatrix} \phi^+ \\ \phi^0 \end{pmatrix} d_R - G_u(\bar{u},\ \bar{d})_L \begin{pmatrix} -\bar{\phi}^0 \\ \phi^- \end{pmatrix} u_R \ +\ hermitian\ coniugate \tag{1.52}$$

In 1.52, the (u, d) quark doublet are considered even if the weak interactions operate on $(u,\ d')_L$ where the primed states are linear combinations of the flavour eigenstates[3]. Using these new doublets, 1.52 is therefore of the form:

$$\mathcal{L} = -G_d^{ij}(\bar{u},\ \bar{d}')_L \begin{pmatrix} \phi^+ \\ \phi^0 \end{pmatrix} d_{jR} - G_u^{ij}(\bar{u},\ \bar{d}')_L \begin{pmatrix} -\bar{\phi}^0 \\ \phi^- \end{pmatrix} u_{jR} \ +\ hermitian\ coniugate \tag{1.53}$$

with i, j = 1, ..., N, where N is the number of quark doublet. Substituting ϕ_c expression, the masses depend on the arbitrary couplings $G_{u,d}$ but, as for electron, it cannot be predicted.
The choose of a particular single Higgs doublet is sufficient on one hand to generate the masses of both of the gauge bosons and the fermions but on the other hand, the masses of the fermoins are just parameteres of the theory and are not predicted.
To summarise, the complete Lagrangian of the SM is:

$$\begin{aligned} \mathcal{L}_{SM} = & \frac{1}{4} W_{\mu\nu} \cdot W^{\mu\nu} - \frac{1}{4} B_{\mu\nu} B^{\mu\nu} + \bar{L}\gamma^\mu (i\partial_\mu - g\frac{1}{2}\tau \cdot W_\mu - g'\frac{Y}{2}B_\mu)L \\ & + \bar{R}\gamma^\mu (i\partial_\mu - g'\frac{Y}{2}B_\mu)R + |i\partial_\mu - g\frac{1}{2}\tau \cdot W_\mu - g'\frac{Y}{2}B_\mu|^2 - V\phi \\ & - (G_1 \bar{L}\phi R + G_2 \bar{L}\phi_c R + \ hermitian\ conjugate) \end{aligned} \tag{1.54}$$

The first two terms represent the $W^\pm$, Z, γ kinetic energies and the self-interactions; the third and the fourth term the lepton and quark kinetic energies and their interaction with weak W, Z and γ; the last terms stand for masses and coupling of the Higgs, bosons, leptons and quark.

1.2 The Higgs boson

The SM Higgs boson is a CP-even scalar of spin 0 [1]. Its mass is given by $m_h = \sqrt{2\lambda\nu^2}$, where λ is the Higgs self-coupling parameter in the potential $V(\phi)$. The experimentally

[3]Linear combination of the flavour eigenstates considering Cabibbo-Kobayashi-Maswaka (CKM) matrix: $d_i' = \sum_{n=1}^{N} V_{in} d_n$ where N = 3 is the number of quarks, V_{in} is CKM matrix and d_n are the d type quarks d, s, b.

Higgs mass, $m_h \simeq 125\ GeV$ [10][11], implies $\lambda \simeq 0.1$ and $|m| \simeq 88.8\ GeV$.
The Higgs boson couplings to the fundamental particles are set by their masses: very weak for light particles, such as up and down quarks, and electrons, but for heavy particles such as the W and Z bosons and the top quark. In particular, the SM Higgs coupling fo fundamental fermions are linearly proportional to the fermion masses. whereas the couplings to bosons are proportional to the squares of the boson masses. As consequence, the dominant mechanism for Higgs boson production and decay involve the coupling of H to W, Z and/or the third generation quarks and leptons. The Higgs boson coupling to gluons is induced at leading order by a one-loop process in which H couples to a virtual $t\bar{t}$ pair. Likewise, the Higgs boson couplings to photons is also generated via loops, although in this case the one-loop graph with a virtual W^+W^- pair provides the dominant contribution and the one involving a virtual $t\bar{t}$ pair is subdominant.

1.2.1 The Higgs boson: production mechanisms

The main production mechanisms at the LHC are gluon fusion, weak-boson fusion, associated production with gauge boson and associated production with a pair of top/antitop quarks. The corresponding Feynman diagrams are reported in Figure 1.2. Figure 1.3

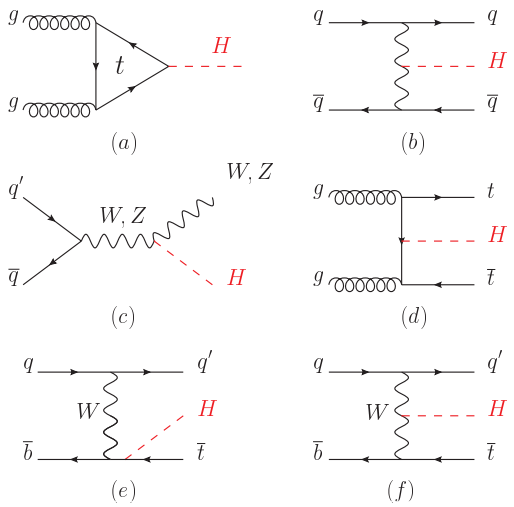

Figure 1.2: Main Leading Order Feynman diagrams contributing to the Higgs production: (a) gluon fusion, (b) Vector-boson fusion, (c) Higgs-strahlung (or associated production with a gauge boson), (d) associated production with a pair of top (or bottom quarks), (e-f) production in association with a single top quark.

summarises these dominant Higgs production processes for a center of mass energy of 13 TeV.

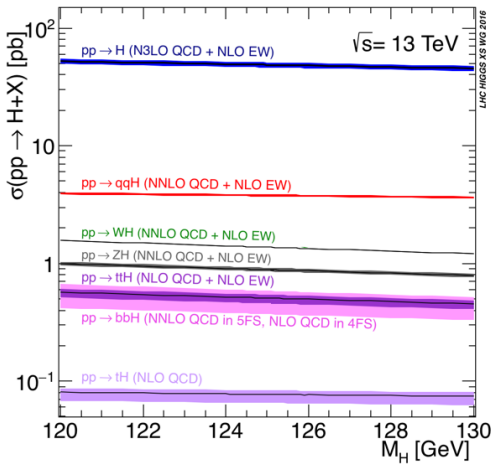

Figure 1.3: Standard Model Higgs boson production cross section at $\sqrt{s} = 13\ TeV$ as a function of Higgs boson mass [12].

Production mechanism: gluon fusion

The Higgs boson production mechanism with the largest cross section is the gluon-fusion process: $gg \to H + X$, mediated by the exchange of a virtual, heavy top quark (Figure 1.2a). Contributions from lighter quarks propagating in the loop are suppressed proportional to m_q^2. QCD radiative corrections to this process are also very important. At the LHC, with a $\sqrt{s} = 13\ TeV$, the value for the production cross section at the next-to next- to next to leading order is [13]:

$$\sigma_{ggF}^{N3LO} = 48.6pb^{+2.2pb(+4.6\%)}_{-3.3pb(+6.7\%)}(theory) \pm 1.6(3.2\%)(PDF + \alpha_s) \tag{1.55}$$

Production mechanism: Weak-boson fusion

The SM Higgs production mode with the second-largest cross section is Vector Boson Fusion (VBF): $qq \to qqH$ (Figure 1.2b). This mechanism proceed by the scattering of two (anti-)quarks, mediated by exchange of a W or Z boson, with the Higgs boson radiated off the weak-boson propagator. The scattered quarks give rise to two hard jets in the forward and backward regions of the detector. Gluon radiation in the central-rapidity is suppressed thanks to the color-singlet nature of the weak-gauge boson exchange: this feature let to distinguish VBF from overwhelming QCD backgrounds including gluon-fusion induced Higgs + 2 jets production and production of H in association with a W or Z boson hadronically decaying. This process receive contributions at NLO from QCD and EW; QCD also contributes at NNLO.

Production mechanism: Higgs-strahlung

The next most relevant Higgs boson production mechanism is the Higgs-strahlung, the production of the Higgs boson with W or Z gauge bosons: $pp \to VH+X$ with $V = W^{\pm}, Z$ (Figure 1.2c). As in VBF, at NLO EW and QCD (due to corrections to the Drell-Yan cross section) give their contributions to this cross section. In addition, Higgs-strahlung receives non Drell-Yan-like conrrections in the $q\bar{q}$ channels where the Higgs is radiated off top-quarks loops.

Production mechanism: ttH

Higgs radiation off top quarks (Figure 1.2d), $pp \to t\bar{t}H$, provides a direct probe of the top-Higgs Yukawa coupling.

1.2.2 The Higgs boson: decay channels

As reported in Figure 1.4, the dominant decay modes for the Higgs boson are $H \to b\bar{b}$, $H \to WW^*$ followed by $H \to \gamma\gamma$, $H \to \tau^+\tau^-$ and $H \to ZZ^*$; Table 1.4 summarises the branching ratios and the relative uncertainty for these decay channels.

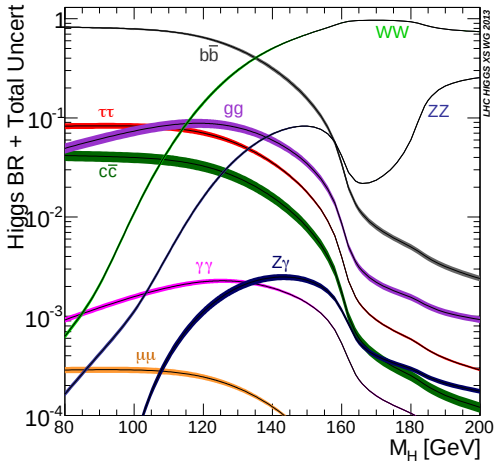

Figure 1.4: Standard Model Higgs boson production cross section at $\sqrt{s} = 13\ TeV$ as a function of Higgs boson mass [12].

Decay channel	Branching ratio	Rel. uncertainty
$H \to b\bar{b}$	$5.84 \times 10^{-}1$	+3.2% -3.3%
$H \to WW^*$	$2.14 \times 10^{-}1$	+4.3% -4.2%
$H \to \tau^+\tau^-$	$6.27 \times 10^{-}2$	+5.7% -5.7%
$H \to ZZ^*$	$2.62 \times 10^{-}2$	+4.3% -4.1%
$H \to \gamma\gamma$	$2.27 \times 10^{-}3$	+5.0% -4.9%
$H \to \mu\mu$	$2.18 \times 10^{-}4$	+6.0% -5.9%

Table 1.4: Standard Model leptons features [14] [15].

Chapter 2

The CMS detector at LHC

2.1 The Large Hadron Collider

Approved in the early '90s and started up in the 2008, the *Large Hadron Collider* is currently the world's largest and most powerful particle accelerator.
Its main purpose is to help in testing the predictions of different theories of particle physics, including the search of the Higgs boson and the dark matter.
Built at a mean depth of 100m, beneath France-Switzerland border near Geneva, in the tunnel formerly used to house the Large Electron-Positron collider (LEP), the LHC of a 26.7km ring of superconducting magnets with a number of accelerating structures to boost the energy of the particles along the way. It is not a perfect circle: it is made of eight arcs and eight 'insertions'. The arcs are long 106.9m with a curvature of 2.84km containing 1232 superconductive dipoles. The LHC dipoles use Niobium-Titanium (NbTi) cables at a temperature of 1.9K, pumping superfluid helium into the magnet system, where they become superconducting; a current of 11850A flows in the dipoles to create the high magnetic field of 8.33 T required to bend the beams around the ring. The insertions instead consist of a long straight section of 528m plus two (one at each end) transition regions. They contains the radiofrequency cavities to increase beam energy (0.5 MeV per period): there are eight cavities per beam, each delivering 2MV (an accelerating field of 5MV/m) at 400MHz operating at 4.5K. Particular kind of insertion are quadrupoles, special magnets used to focus the beam down to the smallest possible size at the collision points: there 392 quadrupoles in LHC.
In the LHC each particle beam is accelerated up to 6.5 TeV (7 TeV is the designed energy not yet reached) but it is the last element of the accelerating chain.
The proton beam is created by using an electric field to pull the electrons from hydrogen atoms and start the acceleration. Protons are injected into the PS Booster (PSB) at an energy of 50 MeV from Linac2 (Linear Accelerator 2). The booster comprises four superposed rings: this is because at low energy intensity, the quality of the beams suffers from the repulsive forces between particles. By splitting up the injected beam this effect gets reduced. Once the beam reaches the energy of 1.4 GeV it is extracted and injected into Proton Synchrotron (PS). With a circumference of 628 m, the PS accelerates the

beams up to 26 GeV when they are extracted and sent to the Super Proton Synchrotron (SPS). Built in the '70, the SPS has a length of 7 km. The beam is injected at 26 GeV, ramped up to 450 GeV and extracted to the LHC. At the SPS, the boson W and Z were discovered and this led Rubbia and Simon van der Meer to win the Nobel prize. In Figure 2.1 a complete scheme of the accelerator chain of the LHC.

Once the energy-working point is reached, the beams are made to collide at four locations

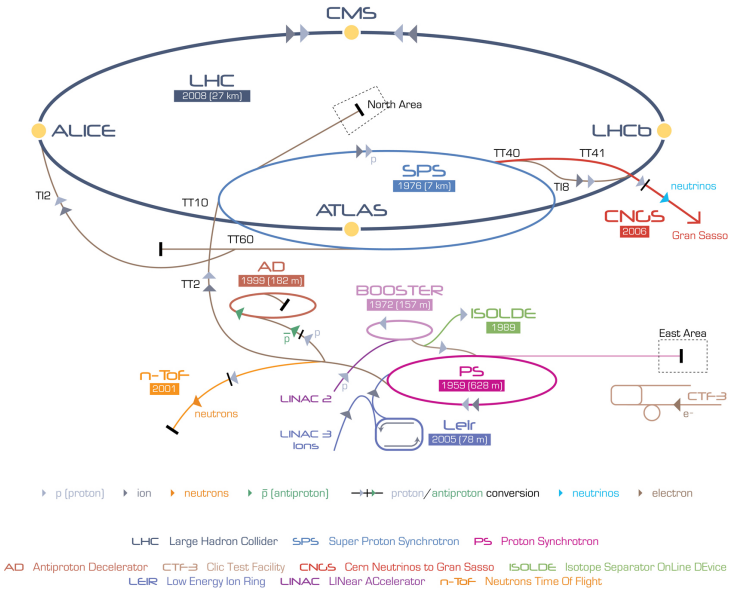

Figure 2.1: Accelerator scheme at CERN.

around the LHC, corresponding to the position of four particles detectors: ALICE (*A Large Ion Collider Experiment*), ATLAS (*A Toroidal LHC ApparatuS*), CMS (*Compact Muon Solenoid*) and LHCb (*Large Hadron Collider beauty*). In addition to these, there are other three experiment installed at the LHC: TOTEM (*TOTal Elastic and diffractive cross section Measurement*) installed close to CMS, MoEDAL (*Monopole and Exotics Detector at the LHC*) close to LHCb and LHCf (*Large Hadron Collider forward*) near ATLAS.

The beams at LHC have a bunch structure as a direct consequence of the radio frequency acceleration scheme. Protons can only be accelerated when the RF field has the correct orientation when particles pass through an accelerating cavity. Under nominal operating conditions, each proton beam has 2808 bunches, with each bunch containing about 10^{11} protons. The bunch size is not constant around the ring getting squeezed as much as possibile around the interaction points in order to increase the probability of collision. They measure a few centimetres long and a millimetre wide when they are far from a collision point; as the bunches approach the collision points, they are squeezed to about 20 μm. LHC uses a bunch spacing of 25 ns (or 7.5 m) corresponding to a frequency of 40 MHz.

High frequency and small beam section, let to increase the number of events, the so call

rate, defined as:

$$\mathcal{R} = \sigma \times \mathcal{L} \tag{2.1}$$

In 2.1, σ represents the cross section of a particular event and $\mathcal{L}$ is the luminosity:

$$\mathcal{L} = \frac{f k_B N_P^2}{4\pi\sigma_x\sigma_y} \tag{2.2}$$

where f is the frequency, k_B the number of bunch and N_P the number of proton in each bunch, σ_x and σ_y instead are the transversal sizes of the bunch at interaction point.
In Table 2.1 are reported the designed LHC parameters and the ones reached at the end of RunII in 2018.

		Design	2018
Centre of mass energy	E	14 TeV	13 TeV
Luminosity	L	10^{34} cm^{-2}s^{-1}	—
Time spacing		25 ns	25 ns
Num. of bunches	k_B	2808	—
Num. protons per bunch	N_p	1.15×10^{11}	—

Table 2.1: LHC parameters

2.2 The Compact Muon Solenoid

CMS, *Compact Muon Solenoid*, is one of the four biggest experiment installed at LHC: it is a general-purpose detector designed to cover the widest possible range of physics at LHC, from precision measurements of the Higgs boson to searches for new physics beyond the Standard Model [16].
In order to manage with these goals, the detector requirements for CMS can be summarised as follows:

- Good muon identification and momentum resolution over a wide range of momenta in the region $|\eta| < 2.5$, good dimuon mass resolution ($\approx 1\%$ at 100 GeV), and the ability to determine unambiguously the charge of muons with p ¡ 1 TeV.

- Good charged particle momentum resolution and reconstruction efficiency in the inner tracker. Efficient triggering and offline tagging of the τ's and b-jets, requiring pixel detectors close to the interaction region.

- Good electromagnetic energy resolution, good diphoton and dielectron mass resolution ($\approx 1\%$ at 100 GeV), wide geometric coverage ($|\eta| < 2.5$), measurement of the direction of the photons and correct localisation of the primary interaction vertex, π^0 rejection and efficienct photon and lepton isolation at high luminosity.

- Good missing transverse energy and dijet mass resolution, requiring hadron calorimeters with a large hermetic geometric coverage ($|\eta| < 5$) and with a fine lateral segmentation ($\Delta\eta \times \Delta\phi < 0.1 \times 0.1$).

The coordinate system adopted by CMS has the origin centered at the nominal collision point inside the experiment, the y-axis pointing vertically upward, and the x-axis pointing radially inward toward the center of the LHC. Thus, the z-axis points along the beam direction toward the Jura mountains from LHC Point 5. The azimuthal angle ϕ is measured from the x-axis in the x-y plane and the radial coordinate in this plane is denoted by r. The polar angle θ is measured from the z-axis. Pseudorapidity is defined as $\eta = -\ln\tan(\theta/2)$. Thus, the momentum and energy transverse to the beam direction, denoted by p_T and E_T , respectively, are computed from the x and y components. The imbalance of energy measured in the transverse plane is denoted by E_T^{miss}.
The overall layout of CMS is shown in Figure 2.2. It is is a 21.6 m long cylinder with a diameter of 14.6 m and a total weight of 12500 tons. At its center sits 13 m long and 5.9 m inner diameter, 4-T superconducting solenoid providing a large bending power (12 Tm); its return field is large enough to saturate 1.5 m of iron, allowing 4 muon stations to be integrated to ensure robustness and full geometric coverage. Each muon station consists of several layers of aluminium drift tube (DT) and resistive pate chambers (RPCs) in the barrel region and cathode strip chambers (CSCs) in the endcap region complemented by RPCs. Inside the magnet coil, the inner tracker and the calorimetry are accommodated. The tracking system is a cylinder of length 5.8 m and a diameter 2.6 m: it consists of 10 layers of silicon microstrip detector plus 3 layers of silicon pixel detectors placed close to the interaction region to improve the measurement of the impact parameter of charged particle tracks as well as the position of the secondary vertices. This configuration provides the required granularity and precision allowing to deal with high track multiplicities. The tracking system is enveloped by the electromagnetic calorimeter (ECAL), made of lead tungstate ($PbWO_4$) crystals with coverage in pseudorapidity up to $|\eta| < 3.0$; in front of the endcap ECAL a preshower system is installed for π^0 rejection. The ECAL is surrounded by a plastic scintillator sampling hadron calorimeter (HCAL) with coverage up to $|\eta| < 3.0$. This central calorimetry is complemented by a "tail-catcher" in the barrel region. Coverage up to a pseudorapidity of 5.0 is provaded by an iron/quartz-fibre calorimeter. The forward calorimeters ensure full geometric coverage for the measurement of the transverse energy in the event.

2.2.1 The tracking system

The tracking system of CMS [17, 18] is designed to provide a precise and efficient measurement of the trajectories of charged particles emerging from the LHC collisions, as well as a precise reconstruction of secondary vertices. It surrounds the interaction point and has a length of 5.8 m and a diameter of 2.5 m. The CMS solenoid provides a homogeneous magnetic field of 4 T over the full volume of the tracker. At the LHC design luminosity of $10^{34} cm^{-2} s^{-1}$ there will be on average about 1000 particles from more than 20 overlapping proton-proton interactions traversing the tracker for each bunch cross-

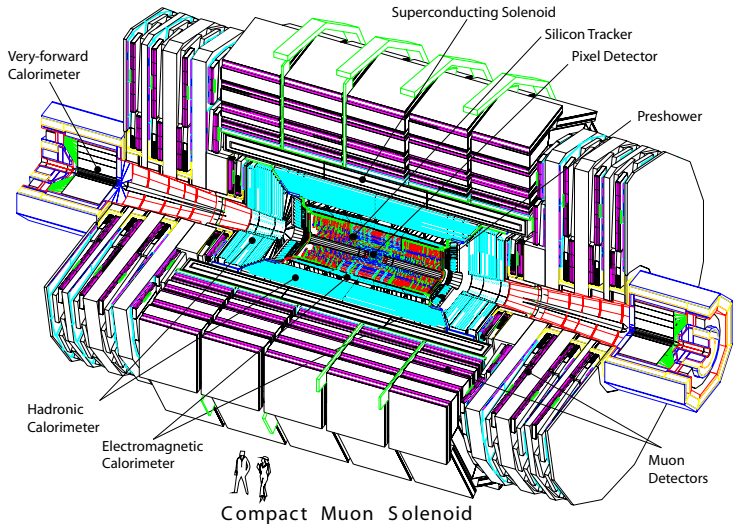

Figure 2.2: CMS detector overview.

ing, i.e. every 25 ns. Therefore a detector technology featuring high granularity and fast response is required, such that the trajectories can be identified reliably and attributed to the correct bunch crossing.
The CMS tracker is shown in Figure 2.3: it is composed of a pixel detector with three barrel layers at radii between 4.4 cm and 10.2 cm and a silicon strip tracker with 10 barrel detection layers extending outwards to a radius of 1.1 m. Each system is completed by endcaps which consist of 2 disks in the pixel detector and 3 plus 9 disks in the strip tracker on each side of the barrel, extending the acceptance of the tracker up to a pseudorapidity of $|\eta| < 2.5$.
The tracker is the closest detector to the interaction point and it has a fundamental role

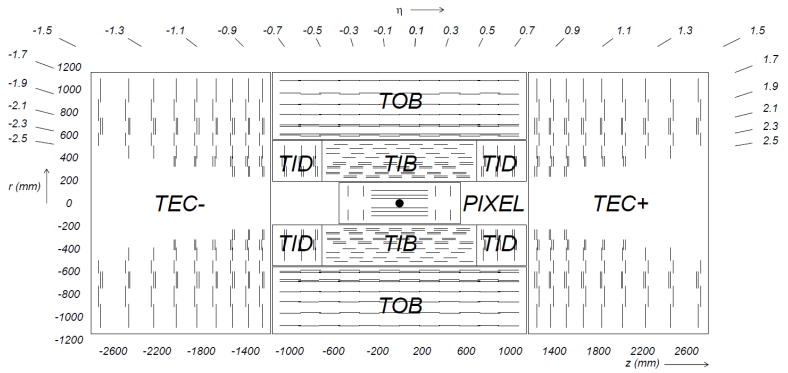

Figure 2.3: Schematic cross section through the CMS tracker in the $r - z$ plane: each line represents a detector module. Double lines indicate back-to-back modules which deliver stereo hits.

in measuring kinematic variables of the particles. In Figure 2.5 is shown the expected resolution of transverse momentum, transverse impact parameter and longitudinal impact parameter, as a function of pseudorapidity for single muons of transerve momentum of 1, 10 and 100 GeV. For high momentum tracks (100 GeV) the transverse momentum

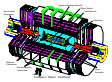

Figure 2.4: Resolution for single muons with transverse momentum of 1, 10 and 100 GeV for several track parameters: transverse momentum (left panel), transverse impact parameter (middle panel), and longitudinal impact parameter (right panel).

resolution is around 1 - 2% up to $|\eta| \approx 1.6$, beyond which it degrades due to the reduced lever arm. At a transverse momentum of 100 GeV multiple scattering in the tracker material accounts for 20 to 30% of the transverse momentum resolution while at lower momentum it is dominated by multiple scattering. The transverse impact parameter resolution reaches 10 μm for high p_T tracks, dominated by the resolution of the first pixel hit, while at lower momentum it is degraded by multiple scattering (similarly for the longitudinal impact parameter). Figure 2.5 shows the expected track reconstruction efficiency of the CMS tracker for single muons as a function of pseudorapidity: the efficiency is about 99% over most of the acceptance and it decreases slightly at $|\eta| \approx 0$ due to gaps between the ladders of the pixel detector at z $\approx$ 0. At high η the efficiency drop is mainly due to the reduced coverage by the pixel forward disks.
MATERIAL BUDGET

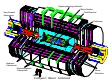

Figure 2.5: Global track reconstruction efficiency for muons of several transverse momentum: 1, 10, 100 GeV.

The pixel detector

The pixel system is the part of the tracking system that is closest to the interaction region and covers a pseudorapidity range $-2.5 < \eta < 2.5$, matching the acceptance of the central tracker. Figure 2.6 shows the geometric pixel strcture as a function of pseudorapidity η. It contributes precise tracking points in $r - \phi$ and z and therefore is responsible for a small impact parameter resolution that is important for good secondary vertex reconstruction. With a pixel cell size of 100×150 μm^2 emphasis has been put on achieving similar track resolution in both $r - \phi$ and z directions: 10 μm in $r - \phi$ direction and 20 μm along z. The pixel detector is essential for the reconstruction of secondary vertices from b and tau decays, and forming seed tracks for the outer track reconstruction and high level triggering. It consists of three barrel layers (BPix) with two endcap disks (FPix). The 53-cm-long BPix layers will be located at mean radii of

4.4, 7.3 and 10.2 cm. The FPix disks extending from ≈ 6 to 15 cm in radius, will be placed on each side at z=±34.5 and z=±46.5 cm. BPix (FPix) contain 48 million (18 million) pixels covering a total area of 0.78 (0.28) m^2. The arrangement of the 3 barrel layers and the forward pixel disks on each side gives 3 tracking points over almost the full ?-range. In the high η region the 2 disk points are combined with the lowest possible radius point from the 4.4 cm barrel layer.

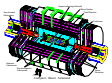

Figure 2.6: Geometrical layout of the pixel detector as a function of pseudorapidity η.

The silicon strip detector

The silicon strip detector is composed of three different subsystem. The Tracker Inner Barrel and Disks (TIB/TID see Figure 2.3) are composed of 4 barrel layers, supplemented by 3 disks at each end. TIB/TID delivers up to 4 $r-\phi$ measurements on a trajectory using 320 μm thick silicon microstrip sensors with their strips parallel to the beam axis in the barrel and radial on the disks. The strip pitch is 80μm on layers 1 and 2 and 120 μm on layers 3 and 4 in the TIB, leading to a single point resolution of 23 μm and 35 μm, respectively. In the TID the mean pitch varies between 100μm and 141μm. The TIB/TID is surrounded by the Tracker Outer Barrel (TOB). It has an outer radius of 116 cm and consists of 6 barrel layers of 500μm thick microstrip sensors with strip pitches of 183μm on the first 4 layers and 122μm on layers 5 and 6. It provides another 6 $r-\phi$ measurements with single point resolution of 53μm and 35μm, respectively. The TOB extends in z between ±118cm. Beyond this z range the Tracker EndCaps (±TEC, where the sign indicates the location along the z axis) cover the region 124 cm ¡ —z— ¡ 282 cm and 22.5 cm ¡ —r— ¡ 113.5 cm. Each TEC is composed of 9 disks, carrying up to 7 rings of silicon microstrip detectors (320μm thick on the inner 4 rings, 500μm thick on rings 5-7) with radial strips of 97μm to 184μm average pitch. Thus, they provide up to 9 ϕ measurements per trajectory. In addition, the modules in the first two layers and rings, respectively, of TIB, TID, and TOB as well as rings 1, 2, and 5 of the TECs carry a second microstrip detector module which is mounted back-to-back with a stereo angle of 100 mrad in order to provide a measurement of the second coordinate (z in the barrel and r on the disks). The achieved single point resolution of this measurement is 230μm and 530μm in TIB and TOB, respectively, and varies with pitch in TID and TEC.
The sensor elements in the strip tracker are single sided p-on-n type silicon micro-strip sensors shown in Figure 2.7: in TIB/TID and on the inner 4 rings of the TECs, thin sensors of (320 ± 20) μm wafer thickness are used, with substrate resistivity of ro = 1.55 - 3.25 kΩcm; TOB and the outer 3 rings of the TECs are equipped with thicker sensors of (500 ± 20) μm thickness, with substrate resistivity of ro = 4 - 8 kΩcm.
LASER ALIGNMENT SYSTEM

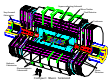

Figure 2.7: Single sided p-on-n type silicon micro-strip sensor.

2.2.2 Electromagnetic calorimeter

The electromagnetic calorimeter of CMS (ECAL) is a hermetic homogeneous calorimeter made of 61200 lead tungstate ($PbWO_4$) crystals mounted in the central barrel part, closed by 7324 crystals in each of the two endcaps. A preshower detector is placed in front of the endcap crystals. Avalanche photodiodes (APDs) are used as photodetectors in the barrel and vacuum phototriodes (VPTs) in the endcaps. The use of high density crystals has allowed the design of a calorimeter which is fast, has fine granularity and is radiation resistant. One of the driving criteria in the design was the capability to detect the decay to two photons of the postulated Higgs boson.

Bibliography

[1] C. Patrignani et al. (Particle Data Group), Chin. Phys. C, 40, 100001 (2016) and 2017 update.

[2] Halzen and Martin, *Quarks and Leptons: An Introductory Course in Modern Particle Physics*, John Wiley & Sons (1984).

[3] M.E.Peskin and D.V.Schroeder, *An Introduction To Quantum Field Theory*, Addison-Wesley, 1995.

[4] M.Maggiore, *A Modern Introduction to Quantum Filed Theory*, Oxford University Press, 2004.

[5] A.Pich, *The standard model of electroweak interactions*, arXiv:hep-ph/0502010v, 2005.

[6] UA1 Collaboration, *Experimental observation of isolated large transverse energy electrons with associated missing energy at sqrts* $= 540\ GeV$.

[7] UA1 Collaboration, *Experimental observation of lepton pairs of invariant mass around* $95\ GeV/c^2$ *at the CERN SPS collider.*

[8] S. Weinberg, *A model of leptons*, Phys. Rev. Lett. 19 (1967) 1264.

[9] MuLan Collaboration, *Improved Measurement of the Positive Muon Lifetime and Determination of the Fermi Constant*, Phys.Rev.Lett.99:032001,2007, arXiv:0704.1981.

[10] ATLAS Collaboration, *Observation of a new particle in the search for the Standard Model Higgs boson with the ATLAS detector at the LHC*, Phys.Lett. B716 (2012), pp. 1-29, DOI: 10.1016/j.physletb.2012.08.020.

[11] CMS Collaboration, *Observation of a new boson at a mass of 125 GeV with the CMS experiment at the LHC*, Physics Letters B716 (2012), pp. 30-61. DOI: http://dx.DOI.org/10.1016/j.physletb.2012.08.021 .

[12] LHC Higgs Cross Section Working Group, https://twiki.cern.ch/twiki/bin/view/LHCPhysics/LHCHXSWG.

[13] D. de Florian et al., [LHC Higgs Cross Section Working Group], CERN-2017-002-M, arXiv:1610.07922[hep-ph] (2016).

[14] S. Heinemeyer et al., [LHC Higgs Cross Section Working Group], CERN?2013?004, arXiv:1307.1347 [hep-ph] (2013).

[15] D. de Florian et al., [LHC Higgs Cross Section Working Group], CERN?2017?002-M, arXiv:1610.07922[hep-ph] (2016).

[16] CMS collaboration, [The Compact Muon Solenoid technical proposal], CERN-LHCC-94-38, http://cdsweb.cern.ch/record/290969

[17] CMS collaboration, [The CMS tracker system project: technical design report], CERN-LHCC-98-006, http://cdsweb.cern.ch/record/368412.

[18] CMS collaboration, The CMS tracker: addendum to the technical design report, CERN-LHCC-2000-016, http://cdsweb.cern.ch/record/490194.